Study of loaded versus unloaded measurements in railway track inspection

Wang, Haoyu; Berkers, Jos; van den Hurk, Nick; Layegh, Nasir Farsad

DOI
10.1016/j.measurement.2020.108556

Publication date
2021

Document Version
Final published version

Published in
Measurement: Journal of the International Measurement Confederation

Measurement 169 (2021) 108556

Contents lists available at ScienceDirect

Measurement

journal homepage: www.elsevier.com/locate/measurement

Study of loaded versus unloaded measurements in railway track inspection

Haoyu Wang [a,b,*], Jos Berkers [a], Nick van den Hurk [a], Nasir Farsad Layegh [a]

[a] Fugro B.V., Utrecht, the Netherlands
[b] Delft University of Technology, Delft, the Netherlands

ARTICLE INFO

Keywords:
Track geometry
Track geometry car
Unloaded measurement
Mobile track inspection system
Track longitudinal level

ABSTRACT

To ensure railway operations safe, track geometry parameters, e.g., track gauge, are usually inspected using track geometry cars. The measurement frequency of track geometry cars is low (twice per year) due to high operational costs and track possession. An innovative way to perform track inspection at high frequency and affordable cost is using mobile track inspection systems, which can be easily mounted on passenger or freight trains. Besides track geometry, it also creates a digital copy of railway corridors providing asset managers with the ability to make fully informed decisions on track assets. Differently, the collectors of mobile systems are further away from the axle than track geometry cars, which are regarded as unloaded and loaded measurement respectively. This difference may lead to a discrepancy in measurement results. This paper studies the difference between loaded and unloaded measurements, using experimental and numerical methods. In the experimental research, a section of track was measured using both systems. The track longitudinal level measured using unloaded and loaded methods were compared, and the discrepancy reported. It was found that although the measuring distance can cause discrepancies, the unloaded measurement method still meets the measurement requirement. The largest discrepancies are in track transition zones, which is explained using the numerical method. After that, a case study using the unloaded measurement method is presented, wherein a section of track has been measured every month. The results show the advantages of frequent measurements in track inspections and the potential applications of unloaded track inspections.

1. Introduction

Railway tracks are regularly inspected to assess the track quality and ensure their safe operation [1–3]. The track quality is described by track geometry parameters normally including track gauge, alignment, longitudinal level (also referred to as surface or profile [4], as shown in Fig. 1), cross level, and twist [5–7]. Track geometry tends to drift away from the design geometry as the number of passed tonnage growing [8]. After collection, track geometry parameters are used for the detection of defects depending on the amplitudes. Various thresholds, i.e., the alert limit, intervention limit and immediate action limit, are considered to determine the maintenance actions [9,10,6]. A common way to measure track geometry is to use track geometry cars with dedicated measuring systems [11,12]. Operating costs are high as these cars require track possession, usually locomotive power, a track geometry car crew, railroad engineering staff, a train crew, frequent maintenance, locomotive fuel, and generator fuel; potentially limiting the inspection frequency. Indeed, in most countries, the railway is only inspected two or three times per year. Moreover, for some privately-owned railways, the track geometry cars are unaffordable due to capital and operating expenditure costs (CAPEX and OPEX). As a result, the track quality cannot be (routinely) timely updated, which leads to less accurate evaluation and consequently less effectively maintenance plan.

An alternative, innovative way to perform track inspection is using mobile track inspection systems that can be easily mounted on passenger or freight trains and operate autonomously. Mobile systems require no track procession or extra locomotives so the inspection cost can be significantly reduced and the inspection frequency increased. For instance, the track between Amsterdam and Eindhoven in the Netherlands has been measured every month using this method. While measuring track geometry, the system also creates a digital copy of railway corridors providing asset managers with the ability to make fully informed decisions on all track assets. Fig. 2a shows examples of the track geometry car (a typical Class 1 track geometry train complete with locomotive(s), power car, and the geometry car) and Fig. 2b shows a mobile track inspection system (Rail Infrastructure aLignment

* Corresponding author.
E-mail address: ha.wang@fugro.com (H. Wang).

https://doi.org/10.1016/j.measurement.2020.108556
Received 18 May 2020; Received in revised form 7 August 2020; Accepted 30 September 2020
Available online 6 October 2020

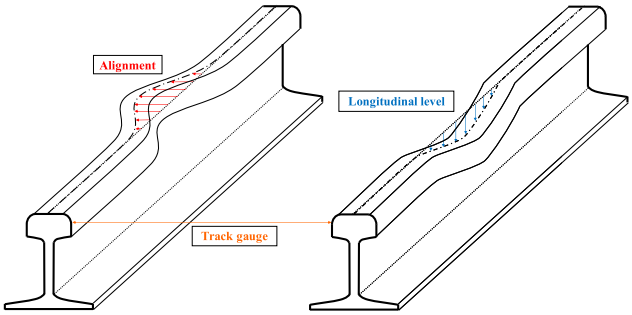

Fig. 1. Explanation of track gauge, alignement and longitudinal level.

Acquisition system, referred to as RILA [13]) mounted on the back of a passenger train respectively.

Both of the measurement systems use laser systems that generate laser lines across the railhead with cross-sectional profiles recorded by high definition cameras [3,4]. The major difference between the two systems is the location of track geometry collectors. In the track geometry car, the collector is positioned between axles of a bogie, relatively close to axles (regarded as loaded measurement, or dynamic measurement). However, the collectors in the mobile track inspection system are mounted to the back of the train body, resulting in a larger distance to axles (regarded as unloaded measurement, or static measurement). The difference in the distance between the collector and axles may lead to a discrepancy in the track geometry measurement results due to the different location at the deflection bowl, especially for the track (surface) longitudinal level as illustrated in Fig. 3.

To use the mobile track inspection system, we need to understand if the measuring distance affects the measurement results, namely, the difference between loaded and unloaded measurements. The goal of this paper is to study the difference between loaded and unloaded measurements in track surveys. The paper is structured as follows. Section 2 describes the measurement device, the sensors and the measuring principle. Section 3 presents the field measurement results of comparing unloaded and loaded methods for a section of the track. In Section 4, a theoretical explanation is provided of the difference between the loaded and unloaded measurements using the Finite Element Method. With a better understanding of the unloaded measurement, a case study is presented in Section 5, wherein the track parameter measured using the unloaded measurement is analysed. Finally, the conclusions are provided in Section 6.

2. Measurement device

The mobile track inspection system comprises a GNSS (Global Navigation Satellite System) antenna, an IMU (Inertial Measurement Unit), a LiDAR (Light Detection And Ranging) scanner, three video cameras, and two laser vision systems (rail scanners) as shown in Fig. 4. All sensors are fixed to the carbon fibre housing unit and the carbon fibre mast - where the GNSS antenna attaches to - is foldable for easy transportation. The detailed sensor parameters are shown in Table 1.

As shown in Table 1, the GNSS position is recorded at 8.89 m intervals along the track at an operating speed of 160 km/h. To improve the accuracy of the GNSS data, the train-collected data is post-processed in conjunction with the data from an active GNSS reference network supplemented with Virtual Reference Stations calculated at 10 km intervals along the track [14] (a network RTK solution). The IMU measures the acceleration and orientation of the system, which is used for post-processing GNSS data. In post-processing step, IMU and GNSS data get integrated, which enables post-processed calculation of intermediate points between primary GNSS positions at 0.148 m intervals. As a result, a high accuracy trajectory solution can be obtained for georeferencing the track data. To further improve the accuracy of the track position, an integrated solution involving the point clouds collected by the LiDAR scanner and the laser vision systems are used. In this step, the track distances between adjacent track lines calculated from the point clouds of the LiDAR scanner are measured accurately and they are used to adjust the position of track data. Also, each survey has been repeated a total of four times to increase the measurement certainty and decrease the effect of stochastic errors, i.e. GNSS related errors. Therefore, a high degree of the absolute accuracy of the track position can be determined without the need for ground control (manual measurements). The standard deviation of the longitudinal and lateral direction of the track (X and Y direction) is less than 8 mm, and that of the vertical direction (Z-direction) is less than 12 mm.

After absolute track geometry data (e.g., track position) is acquired, the track chainage can be calculated and adjusted to the asset database. During the measurement, the relative track geometry is measured by the laser vision systems. The laser vision system projects a laser beam over each rail and, as it passes over, the integrated camera captures high-resolution images of the rail profile. A blue colour laser beam is used to avoid interference of the sunlight, as shown in Fig. 5.

The laser vision system measures the coordinates of more than 1400 laser points per railhead at 500 times per second. Rail profiles are recorded at 9 cm intervals at an operational speed of 160 km/h (100 mph). For each captured laser image of the rail head and rail foot, the wear of the rail can be calculated by comparing it with the reference rail profile. The relative track geometry parameters, for example, gauge and cant, can be calculated by combining the laser images of two rails. An example of a single rail profile is shown in Fig. 6a, where the green line is the reference rail profile, the black dots are the rail profile captured by the laser vision system, and the wear is indicated by the red arrows. The measurement results of a switch (turnout) combined by multiple rail

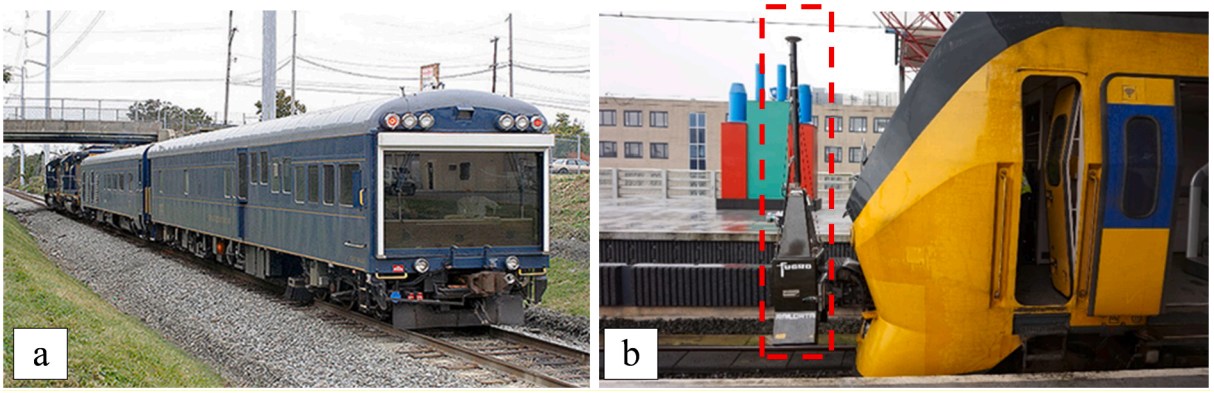

Fig. 2. Typical Class 1 track geometry train complete with locomotive(s), power car, and the track geometry car (a); Mobile track inspection system-RILA mounted on the back of a passenger train (b).

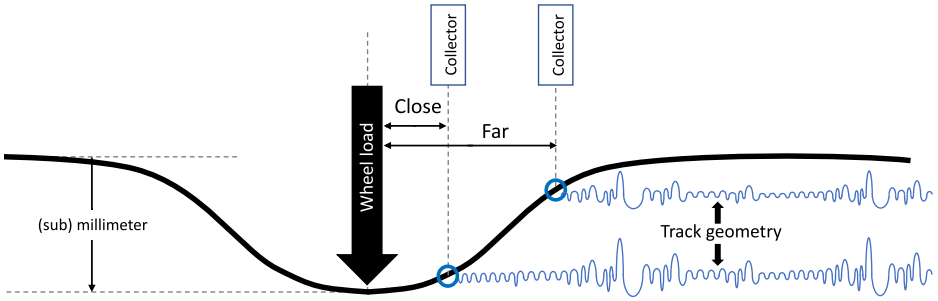

Fig. 3. Schematic diagram of the difference caused by the distance between collector and axle.

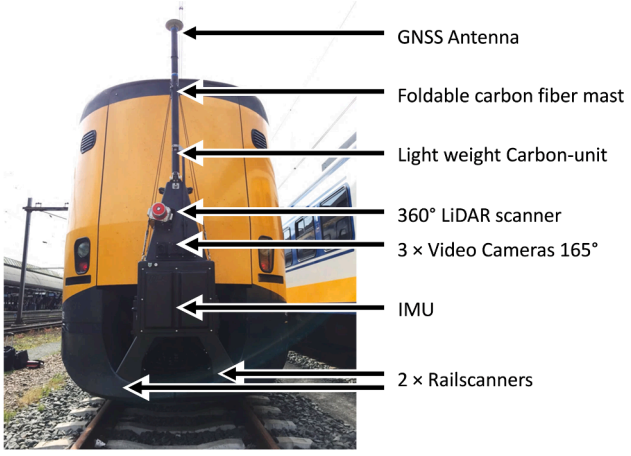

Fig. 4. Mobile track inspection system (Rail Infrastructure aLignment Acquisition system, referred to as RILA).

Table 1
Parameters of sensors.

	Sampling frequency (Hz)	Amount	Sampling interval along the track (m)	
			at 100 km/h (62 mph)	at 160 km/h (100 mph)
GNSS antenna	5	1	5.56	8.89
IMU	300	1	0.09	0.15
LiDAR scanner	250 × 4000[1]	1	0.11	0.18
Laser vision system	500 × 2352[2]	2	0.06	0.09
Video camera	15	3	1.85	2.96

[1] 250 rounds per second and 4000 points per round.
[2] 500 rail profiles per second and 2352 points per profile.

profiles are shown in Fig. 6b.

One of the advantages of the mobile track inspection system is that it can be easily attached to any passenger or freight train. It is commonly installed on the automatic couplers on the rear of a train via a custom-built adaptor. The installation can be conducted in one or two minutes during a regular train stop. Throughout the installation process, two operatives need to step in the track, with the permission received from the train operating company or railway company. After installation, the two operatives travel on the train in the rear driver's cabin. The installation process is shown in Fig. 7. It is remarkable to note that the measurement results are less affected by the weather during operation because the device is normally mounted to the rear of trains.

3. Experimental analysis

To study whether the measuring distance affects the measurement results, a field measurement was performed on the track between Den Haag and Zoetermeer, in the Netherlands as shown in Fig. 8a (the measured track is indicated by the green line). The track is a standard ballast track with double tracks consisting of 30 cm-depth ballast bed, concrete sleepers (ties) and UIC54 rails. More information regarding the measurement is provided in [15] Because the track longitudinal level measures the deviation in the vertical direction of the running surface on rails from the smoothed vertical position, which indicates the vertical smoothness of a track, it is most sensitive to the distance issue, as illustrated in Fig. 3. It is analysed with a relatively short wavelength (between 3 m and 25 m, D1 band in [5]) in this section. It should be noted the track longitudinal level is a relative result calculated from the absolute result - track elevation. During the calculation, a bandpass filter and a 4th order Butterworth filter is used, according to [5].

During the measurement, the mobile track inspection system was installed on a locomotive at a close location (1.1 m), and a far location (3.1 m) separately, as the schematic diagram shown in Fig. 8b. The wheel load of the locomotive is 8.5 ton. The close and far location are regarded as loaded and unloaded respectively according to EU standards [5]).

The track longitudinal level was measured using the system in both the close and far position. In total 6 runs were performed. The detailed parameters of runs are shown in Table 2.

The measurements were performed under similar conditions on a 3 km long section of track and conducted on the same day. By comparing the measurement results with the same measuring distance, e.g., Run 1and Run 3, the stability of the device can be analysed, which is referred to as repeatability [12]. On the other hand, by comparing the results measured with different measuring distance, e.g., Run 1 and Run 5, the effect of measuring distance can be analysed, which is referred to as reproducibility. Therefore, the four tests can be arranged as shown in Table 3.

The results of the tests are shown in Fig. 9a–h. In the figure, we first compared the measurement results and then calculated the discrepancies (absolute value). According to [12], the 95 percentile of the discrepancies is used as an indicator evaluate the repeatability and reproducibility of the device, the limits of which are 0.5 mm and 0.8 mm, respectively. The histograms of the tests are shown in Fig. 10.

As shown in Fig. 9a and c, the results from those runs with the same conditions are very close indicating that the repeatability of the measurement is good. The discrepancies between the two measurements (see Fig. 9b and d) are also very low. On the contrary, the discrepancies between the loaded and unloaded measurements are relatively larger as shown by Test 3 and Test 4 (Fig. 9e–h). The statistical analysis of tests is shown in Table 4. Although the measuring distance increases the discrepancies, the 95 percentile of the discrepancies are still smaller than the limit – 0.8 mm, meaning the difference between the loaded and

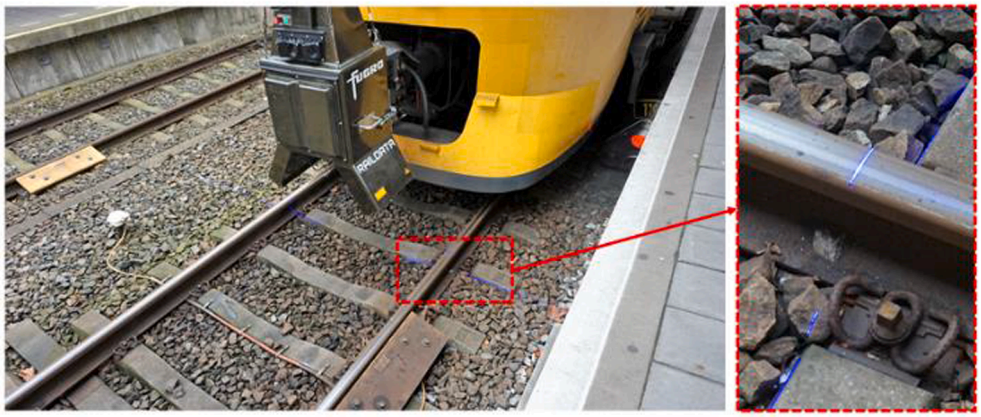

Fig. 5. Laser beam of the laser vision system.

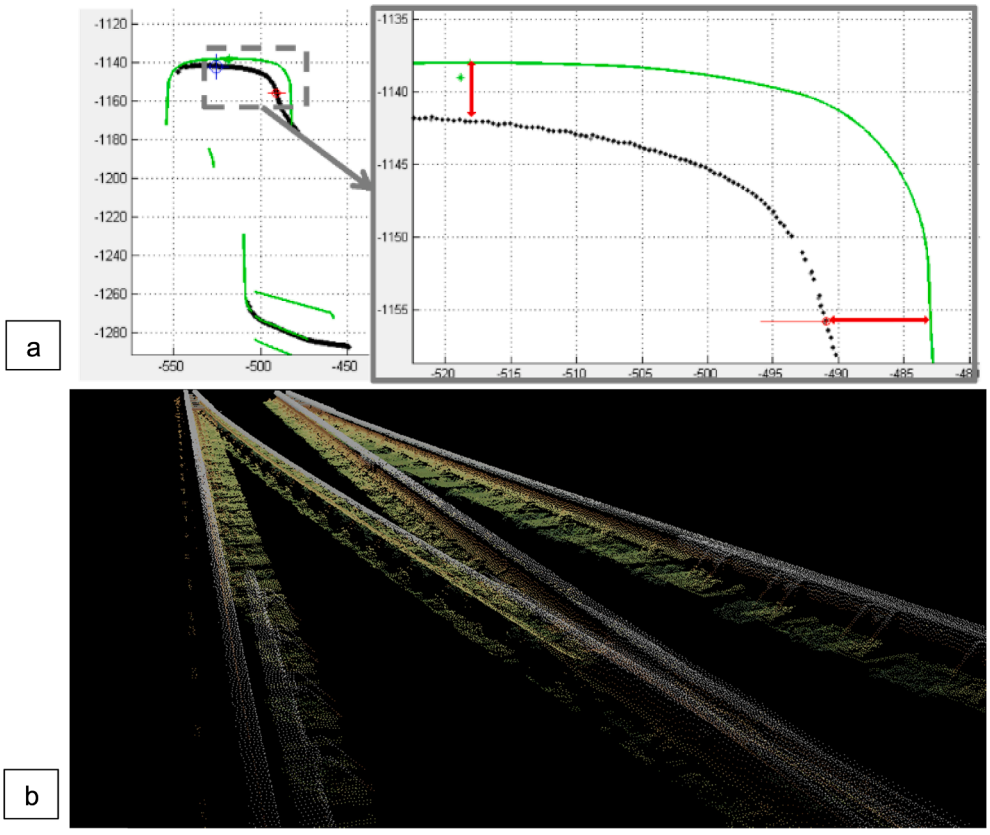

Fig. 6. Measurement results of laser vision system: Rail cross-section [mm] (a); Switch profile (b).

unloaded measurements are small.

The repeatability of measurement (measurement error) can be estimated using the 95 percentile of Test 1 and Test 2 in Table 4, which is 0.07–0.15 mm. Taking into consideration that the discrepancies in Test 3 and 4 contain both the measuring distance effect and measurement error, the result of measuring distance can be approximated as 0.12–0.27 mm. Comparing to the limit of reproducibility 0.8 mm, the discrepancies between the loaded and unloaded measurements are small, which are 0.27–0.34 mm. We can therefore conclude that although the unloaded measurements cause minor discrepancies they produce satisfactory results.

Another finding from the results is that the discrepancies between the loaded and unloaded measurements are significantly unevenly distributed; the majority are small values but some are considerable. For instance, 95 percentile of the discrepancies of Test 4 is less than 0.27 mm, while the maximal discrepancy reaches 1.13 mm (unloaded measurement is less than loaded measurement). This may mean the effect of measuring distance becomes more significant in some specific locations than others. To validate the assumption, the corresponding location of the maximal discrepancy of Test 3 and Test 4 (18.431 km and 18.408 km, respectively), as indicated by P1 in Fig. 9f and P2 in Fig. 9g, are marked on the map as shown in Fig. 11.

As shown in Fig. 11, the main discrepancy in both Test 3 and Test 4 appears in the same bridge transition zone at the bridge-embankment transition (when the train leaves the bridge) indicating that measuring distance has an effect on the track geometry measurement in track transition zones. The reason for this may be related to the severe track geometry irregularity often observed in transition zones [16–20], e.g.,

Fig. 7. Installation of mobile track inspection system: Install coupler adapter to train coupler (a); Install the measurement system to coupler adapter (b); Unfold antenna (c); Leave track (d).

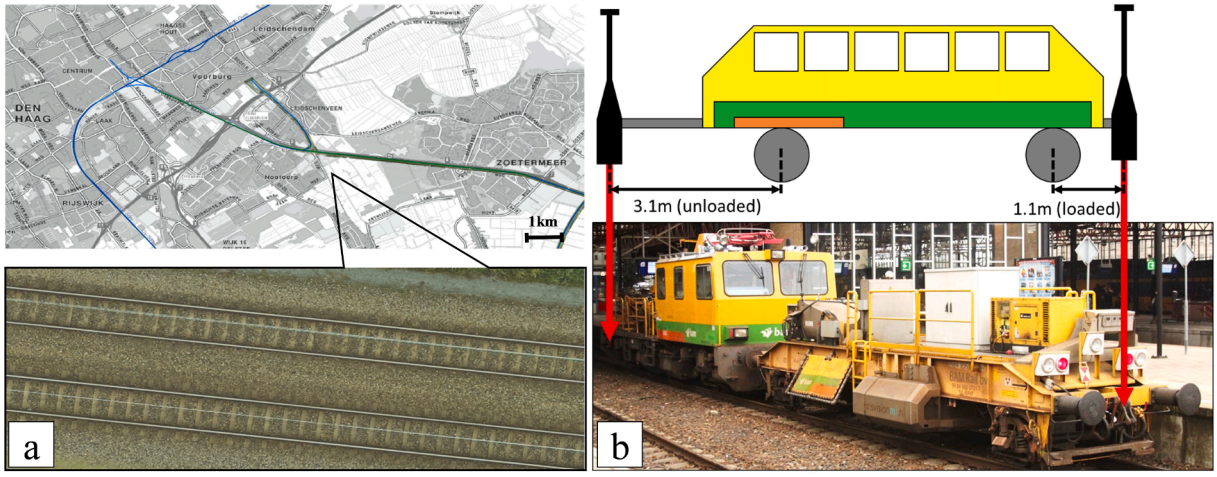

Fig. 8. Location of field measurement (a); Measurement locomotive (b).

Table 2
Run parameters.

Run No.	Distance	Moving direct
1	Close	←[1]
2	Close	→[2]
3	Close	←
4	Far	→
5	Far	←
6	Far	→

[1] ← means the train moves from Zoetermeer (East) to Den Haag (West).
[2] → means the train moves from Den Haag (West) to Zoetemeer (East).

hanging sleepers (the sleepers poorly supported by ballast but hanging to rails). This phenomenon is studied in detail under Section 4 using numerical simulation.

Table 3
Test setup.

Test No.	Runs included	Representation	Name
1	1, 3	Measurement error	Repeatability
2	4, 6		
3	1, 5	Distance effect + Measurement error	Reproducibility
4	2, 4		

4. Numerical analysis

To analyse the effect of the measuring distance in track transition zones, a theoretical study was performed using the Finite Element (FE) method. The dynamic model used is shown in Fig. 12a. The model consists of three main parts, namely two ballast tracks on the

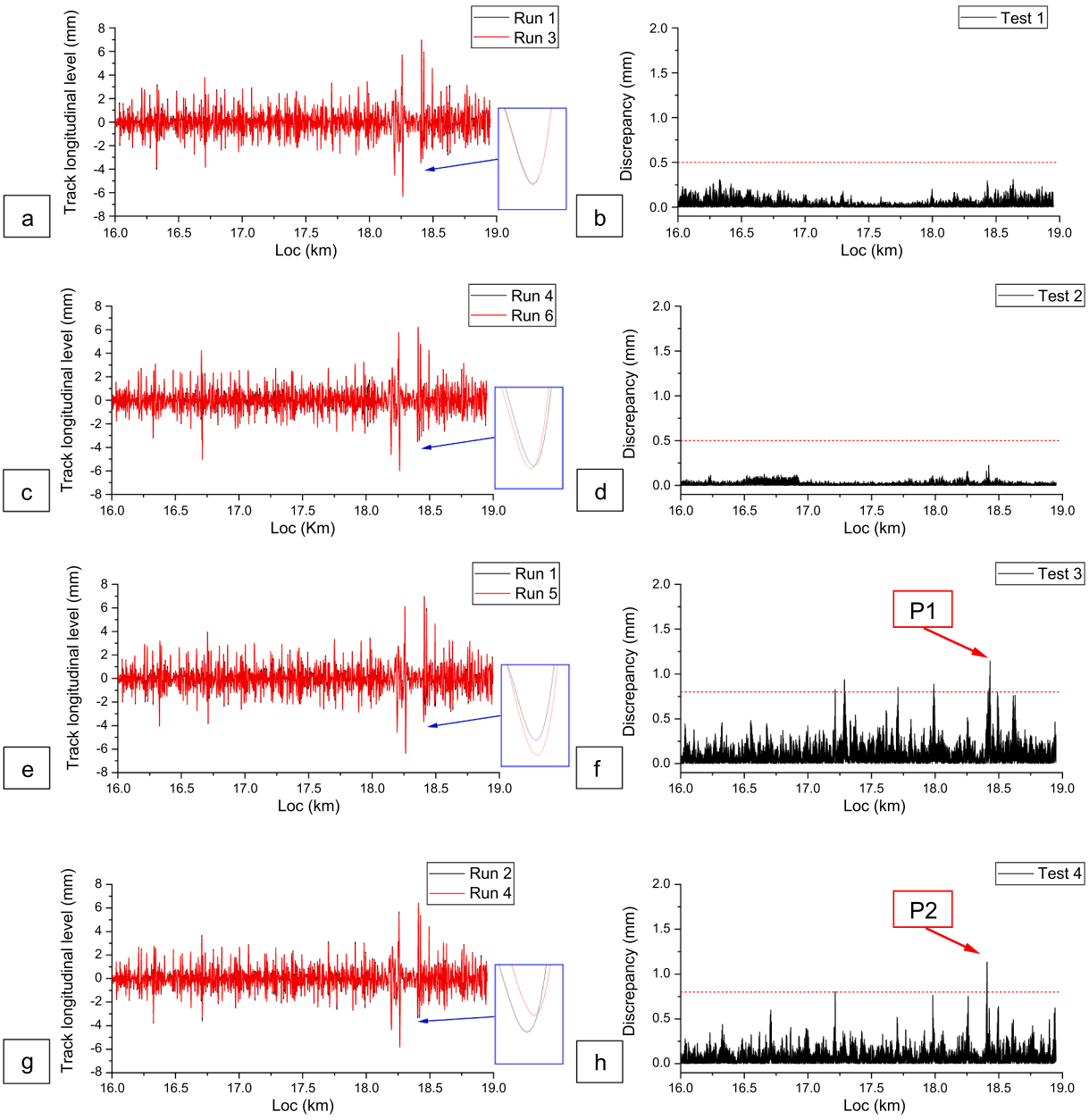

Fig. 9. Comparison of the track longitudinal level measured in Run 1 and Run 3, Test 1 (a); Discrepancy between Run 1 and Run 3, Test 1 (b); Comparison of the track longitudinal level measured in Run 4 and Run 6, Test 2 (c); Discrepancy between Run 4 and Run 6, Test 2 (d); Comparison of the track longitudinal level measured in Run 1 and Run 5, Test 3 (e); Discrepancy between Run 1 and Run 5, Test 3 (f); Comparison of the track longitudinal level measured in Run 2 and Run 4, Test 4 (g); Discrepancy between Run 2 and Run 4, Test 4 (h).

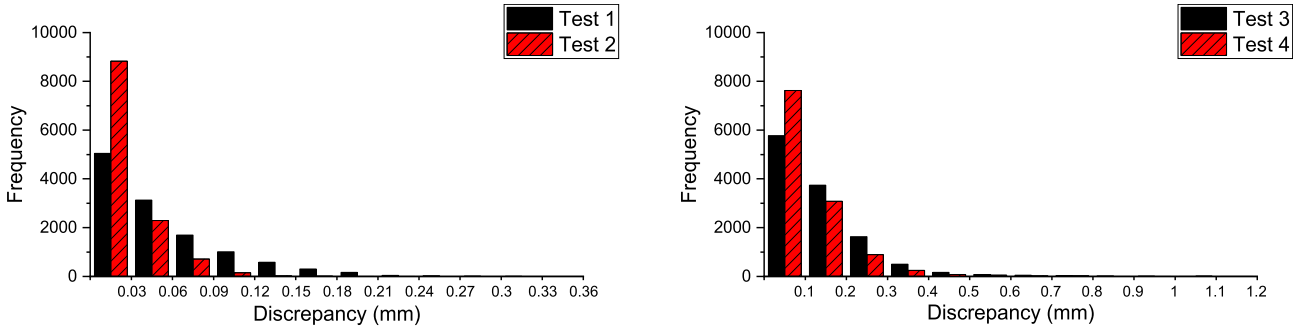

Fig. 10. Histogram of Test 1 and Test 2 (a); Histogram of Test 3 and Test 4 (b).

Table 4
Statistics analysis of tests.

Test No.	Representation	Average (mm)	95 percentile (mm)	Maximum (mm)
1	Measurement error	0.05	0.15	0.31
2		0.02	0.07	0.22
3	Distance effect +	0.13	0.34	1.15
4	Measurement error	0.10	0.27	1.13

embankment and a slab track on a bridge. The ballast tracks are both 48 m long, and the bridge section is 24 m long. The total length of the model is 120 m. The vehicle model is 23 m long, moving from the one end of the track to the other end at the velocity 140 km/h. The components of ballast tracks are rails, fasteners, sleepers, and ballast. The rails are modelled by Hughes-Liu beam elements with 2*2 Gauss quadrature integration [21]. The cross-sectional and mass properties of the UIC54 rails are used and the element length of rail is 75 mm. Spring-damper elements between rails and sleepers are used to simulate fasteners. Sleepers and ballast are modelled by three-dimensional elastic bodies which are composed of the selective reduced integrated hexahedral solid

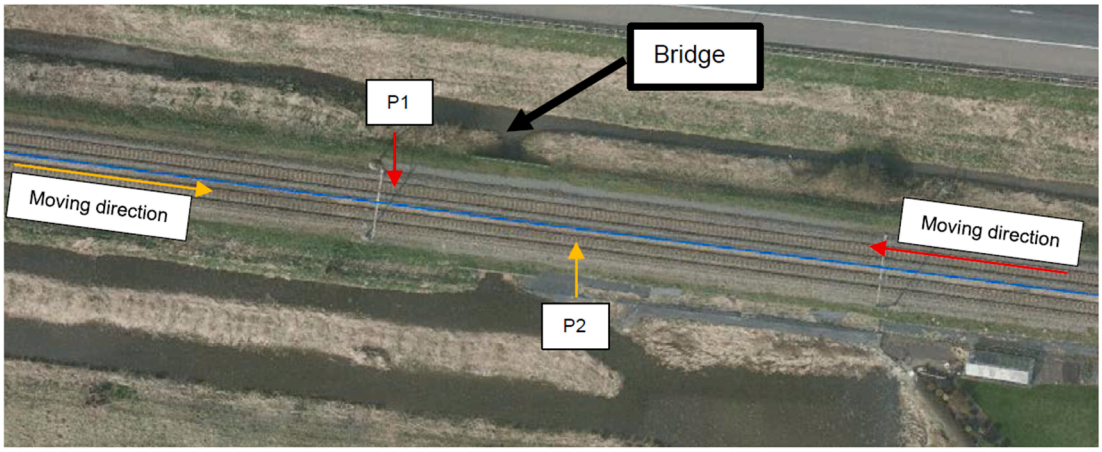

Fig. 11. Track section corresponding to maximal discrepancies, P1 from and P2 from Fig. 9.

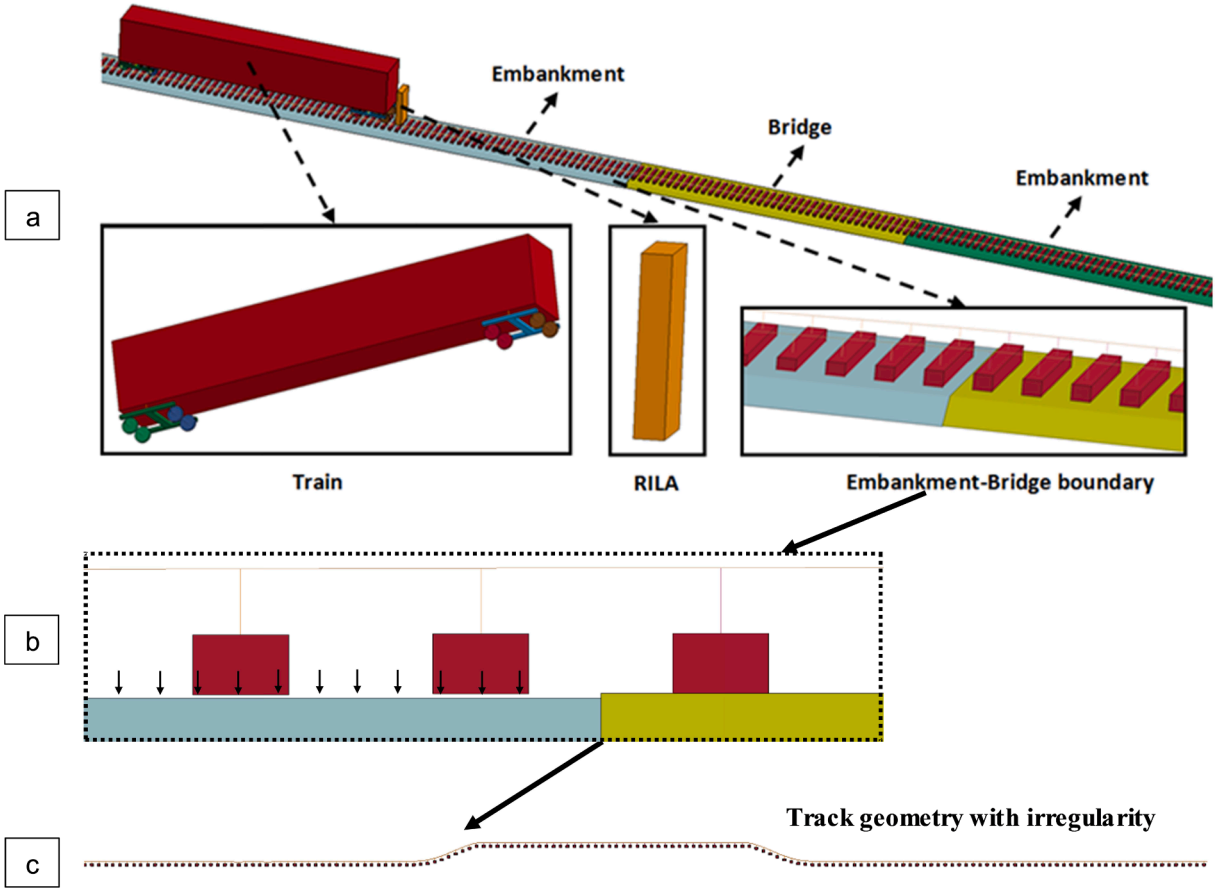

Fig. 12. FE model of train and track (a); Track geometry with irregularity in transition zone model (b); Track geometry with irregularity, enlarged by 30 times (c).

elements. The vehicle model is idealised as a multibody system consisting of one carbody, two bogies and four wheelsets. The primary and secondary suspensions are modelled by spring-damper elements.

The contact between wheel and rail is modelled using the Hertzian spring and the connection between sleepers and ballast is modelled by nonlinear contact elements, which enables the separation between sleepers and ballast so that the spatial movement of hanging sleepers can be modelled more accurately. The non-reflecting boundary conditions are applied on both ends of the model to reduce the wave reflection effect [22]. The bottoms of the ballast and the bridge are fixed. The detailed parameters of the model are shown in Table 5 and the model has been validated [23].

To model the track geometry irregularity in the transition zone, a downwards differential settlement is added to the embankment, while the track on the bridge remains unchanged, as shown in Fig. 12b. The differential settlement used here is 8 mm, which is often found in field measurements e.g., in [24]. After adding the differential settlement, the track geometry is indicated in Fig. 12c (enlarged 30 times). Some sleepers next to the bridge are hanging due to the differential settlement and the constraint of the track on bridge.

The mobile track inspection system is modelled by a rigid body element with lightweight. It has the same velocity as the vehicle but is disconnected from the vehicle to ensure it isn't affected by train vibration. During the simulation, the vertical coordinate of the collecting point of the inspection system is recorded, regarded as the track longitudinal level measured by the inspection system model. The model of the inspection system is placed at the close location (1.1 m) and the far location (3.1 m) respectively as per the field measurements (Section 3). The calculated track longitudinal level (D1) are compared at two locations in Fig. 13.

As shown in Fig. 13, the results are very similar in the track sections on the embankment (before 45 m and after 85 m) as well as in the section on the bridge (from 56 m to 74 m). Considering the track sections on the embankment having a lowing track stiffness and that on the bridge high, it shows that the loaded and unloaded measurements producing the same results as long as the track stiffness is constant.

On the contrary, relatively large discrepancies have been found on the track section with stiffness variation, i.e., the transition zone from embankment (from 45 m to 55 m) the bridge and from the bridge to the embankment (from 75 m to 85 m). Especially, the results of the unloaded measurement account for 83.6% of the loaded results, which means more than 15% value lost. The bottom values of the loaded and unloaded case are −4.23 mm and −5.06 mm respectively. The numerical results correlate strongly with those in the field as shown by the comparison of discrepancies in Fig. 14.

As shown in Fig. 14, discrepancies can be found both before and after the bridge in the transition zone, wherein the one in the bridge-embankment transition (train moving off the bridge) is larger. It can

Table 5
Parameters of the transition zone model.

Parameter	Value
Axle load (kN)	186.3
Distance between wheels (m)	2.5
Distance between bogie centres (m)	20.0
Length of carbody (m)	23.0
Primary suspension stiffness (N/m)	4.25 × 10^10
Primary suspension damping (Ns/m)	1.8 × 10^10
Secondary suspension stiffness (N/m)	4.68 × 10^10
Secondary suspension damping (Ns/m)	3.5 × 10^10
Secondary suspension bending stiffness (Nm/rad)	1.05 × 10^10
Elastic Modulus of sleeper (Pa)	3.65 × 10^10
Poisson ratio of sleeper	0.167
Elastic Modulus of ballast (Pa)	1.20 × 10^10
Poisson ratio of ballast	0.25
Elastic Modulus of concrete slab (Pa)	3.50 × 10^10
Poisson ratio of concrete slab	0.167

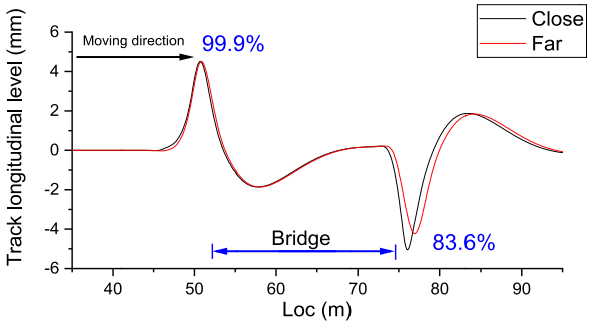

Fig. 13. Simulation results of the track longitudinal level collected at the close and far points.

also be seen that the discrepancy curve of the measurements taken in the field fluctuates more compared to that of the simulation. This proves that the loaded and unloaded measurements have very similar results when the track has even stiffness, while having discrepancies only when the track has stiffness variation.

The reason for large discrepancies appearing in transition zones can be explained by the 'hidden' track irregularity (or dynamic track irregularity) which only appears under loading, e.g., hanging sleepers in transition zones. Given that the track stiffness is even, the measurement results using loaded or unloaded measurement should be the same. When the track stiffness becomes low on short sections, for example, due to a hanging sleeper, the unloaded measurement captures a smaller value than the loaded measurement because the collector has a longer distance to the bottom of the deflection bowl. It should be noted that the discrepancy is minor; 16.7% according to the simulation results. Also, since the wheel-rail contact point represents the bottom of the deflection bowl, even the loaded measurement is a distance from it and therefore also has a certain reduction compared to the true value. As a result, when comparing the unloaded measurement with loaded measurement, we are not comparing a 'reduced' value with a 'true' value, but a 'relatively more reduced' value with a 'relatively less reduced' value. In addition, the difference between them only appears when the track has a local stiffness variation. Also, the maximum reduction is less than 20% (16.7%), which is insignificant.

Considering the findings that the largest reduction is insignificant, and that the results of the unloaded measurement meet the required measurement standards (see Section 3), it is recommended to use the unloaded measurement method as it has many advantages in terms of cost reduction and increasing the measurement frequency.

5. Case study

With a better understanding of the unloaded measurement method, a case study of using it to measure the track geometry has been conducted. A section of the passenger railway line between Amsterdam and Eindhoven has been measured monthly using the mobile track inspection system. The whole track has been measured five times, including August 2018, September 2018, October 2018, November 2018, and January 2019. December 2018 is unfortunately not measured due to practical reason. The track longitudinal level (D1) in a representative location is analysed in Fig. 15a.

As seen in Fig. 15a, the longitudinal levels of the 5 runs are similar to each other before 20.5 km and after 23 km but between these values is a relatively large variation. The largest change appears at 21.85 km, which can be seen in Fig. 15b; the amplitudes increase from September 2018 reaching the maximum level in November 2018, while reduces in January 2019. The standard deviation of the longitudinal level is calculated using a 25 m sliding window (100 samples) following the method used in [25], as shown in Fig. 16a.

Similar to Fig. 15a, Fig. 16a shows that the standard deviation is

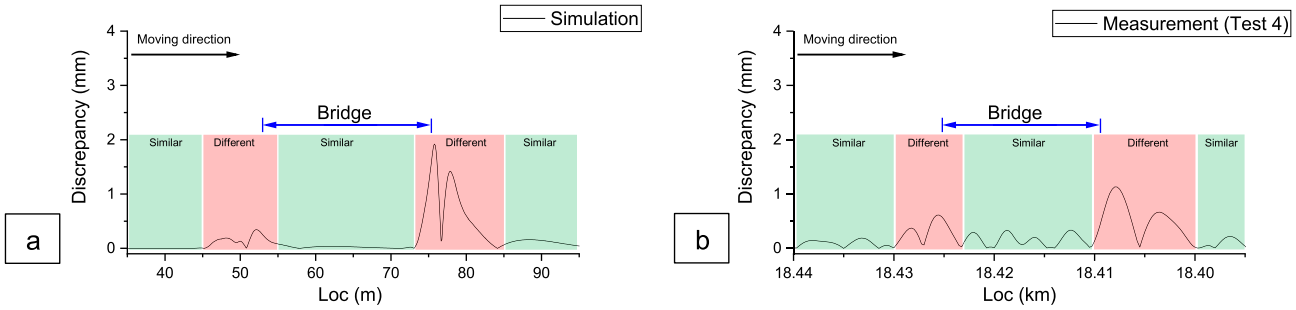

Fig. 14. Discrepancy between the results of track longitudinal level at close and far: Simulation (a); Measurement (b), zoom-in from Fig. 9h.

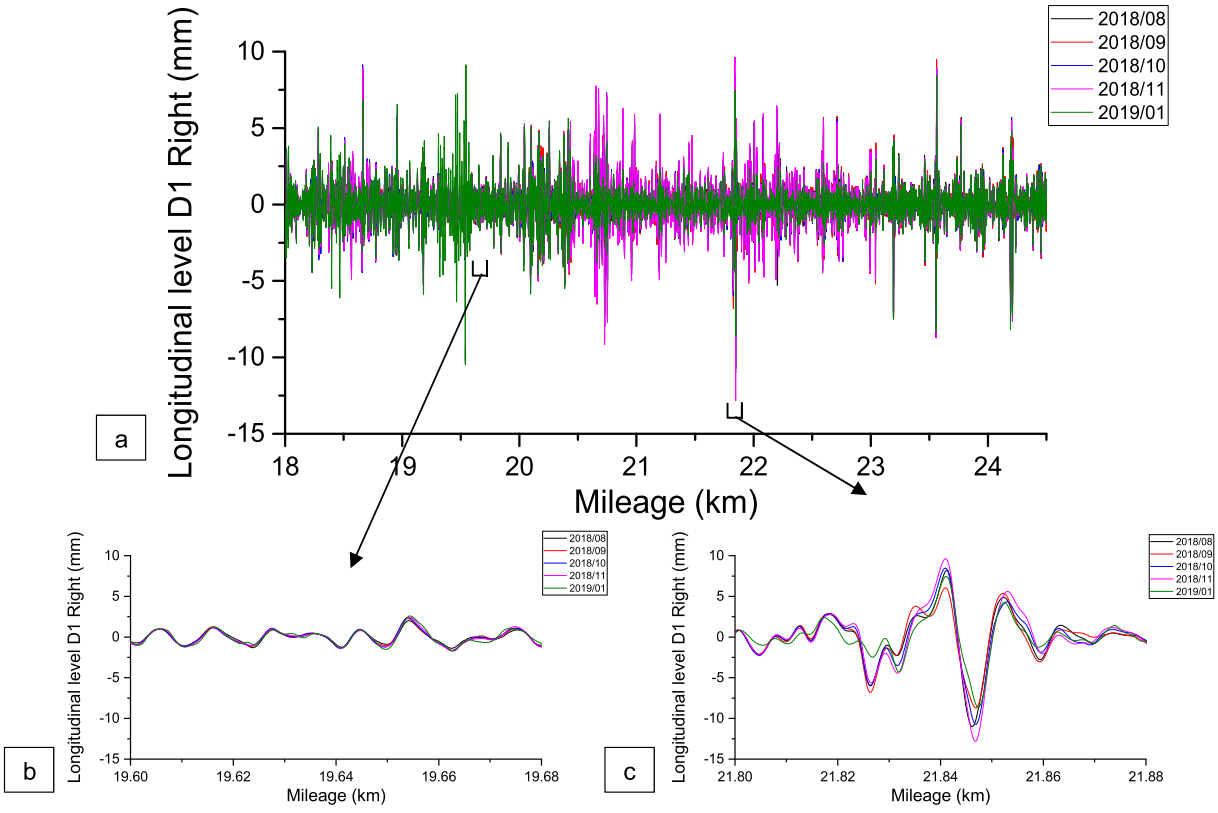

Fig. 15. Measured track longitudinal level of 5 runs: Overview (a); Zoom-in km 19.60–19.68 (b); Zoom-in km 21.80–21.88 (c).

higher at 20.7 km, 21.8 km and 24.2 km than at other locations. Fig. 16b shows the detailed change of the standard deviation overtime at 21.8 km, revealing the local degradation process of the track quality. The standard deviation is reduced in January 2019, indicating that maintenance was performed between November 2018 and January 2019. After consulting with the railway owner (ProRail), it was confirmed that a track maintenance was performed in December 2018. It should be noted that the quality of the track for those locations with a high standard deviation is poor and remains poor even after maintenance, confirming the 'memory effect' of track [26,3,27]. The reason for the fast degradation is due to poor subgrade confirmed by the maintenance staff.

Fig. 17 shows the average standard deviation of the longitudinal level D1 over the entire track section. The increase rate can be calculated (indicated by the red solid line), reflecting the rate of track degradation. Moreover, the effect of maintenance can be seen by the vertical dotted line. This information can provide a deeper understanding for the maintenance staff to evaluate the track quality and the maintenance performance, which cannot be captured when the track is measured at the conventional frequency (twice per year).

6. Conclusions

This paper presents an innovative approach to perform track inspection. The method uses a mobile track inspection system (RILA) which can significantly reduce the inspection cost and increased the inspection frequency. Since the system is mounted to the end of passenger or freight trains, its collector has a longer distance to the bottom of the track deflection bowl (wheel-rail contact point) comparing to track geometry cars. Thus, it is regarded as an unloaded measurement. The paper studied the effect of the measuring distance on track geometry measurement, in both experimental and numerical ways.

The field measurement shows that the device has good repeatability and reproducibility. Although the measuring distance can cause relatively small discrepancies, the unloaded measurement method still meets the requirement of measurement standard. Another finding from the field measurement is that the discrepancies between the loaded and unloaded measurements are significantly unevenly distributed. The largest discrepancies are found in transition zones (the bridge-embankment transition), where the larger stiffness variation and

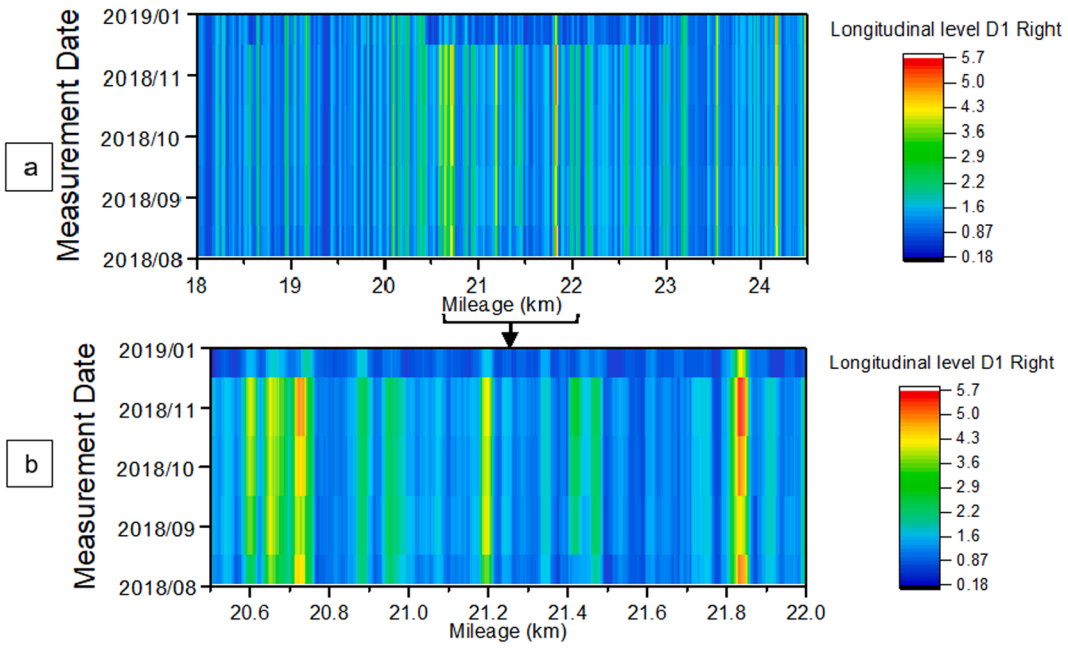

Fig. 16. Standard deviation of longitudinal level: Overview (a); Zoom-in (b).

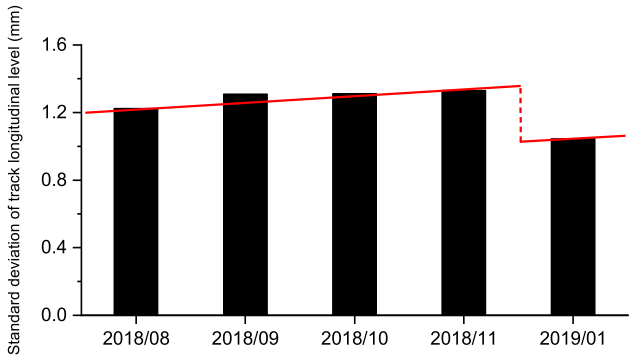

Fig. 17. Average standard deviation of track longitudinal level.

differential settlement appears.

The results numerical simulation shows that the measurement results using loaded or unloaded measurement should be very similar, given that the track stiffness is even. When the track stiffness varies at short section, e.g., due to a hanging sleeper, the unloaded measurement captures a smaller value than the loaded measurement. The largest discrepancy is also found in the bridge-embankment transition, where the unloaded measurement captures 80% of the amount of the loaded measurement.

Because the effect of the measuring distance is small, it is recommended to use the method to increase the measurement frequency, e.g., from once per 6 months to once per month. The frequent measurement results show a very detailed track degradation process and the effectiveness of the track maintenance.

CRediT authorship contribution statement

Haoyu Wang: Conceptualization, Methodology, Software, Data curation, Writing - original draft. **Jos Berkers:** Conceptualization, Methodology, Supervision. **Nick van den Hurk:** Conceptualization, Supervision. **Nasir Farsad Layegh:** Data curation.

Declaration of Competing Interest

The authors declare that they have no known competing financial interests or personal relationships that could have appeared to influence the work reported in this paper.

Acknowledgement

The authors would like to sincerely thank Eric van den Bosch for making the report of Validatie RILA-S&C module. The authors are very grateful to all reviewers for their thorough reading of the manuscript and constructive comments.

References

[1] Y. Wang, P. Wang, X. Wang, X. Liu, Position synchronization for track geometry inspection data via big-data fusion and incremental learning, Transp. Res. Part C Emerg. Technol. 93 (June) (2018) 544–565.
[2] L.M. Quiroga, E. Schnieder, Monte Carlo simulation of railway track geometry deterioration and restoration, Proc. Inst. Mech. Eng. Part O J. Risk Reliab. 226 (3) (2012) 274–282.
[3] C. Esveld, Modern railway track. (2001).
[4] W.T. McCarthy, Track geometry measurement on Burlington Northern Railroad, Nondestruct. Eval. Aging Railr. 2458 (June 1995) (2004) 148–164.
[5] CEN (European Committee for Standardization), EN 13848-1 Railway applications-Track-Track geometry quality-Part 1: Characterisation of track geometry, 2019.
[6] A. Haigermoser, B. Luber, J. Rauh, G. Gräfe, Road and track irregularities: measurement, assessment and simulation, Veh. Syst. Dyn. 53 (7) (2015) 878–957.
[7] J. Sadeghi, Development of railway track geometry indexes based on statistical distribution of geometry data, J. Transp. Eng. 136 (8) (2010) 693–700.
[8] P.F. Weston, C.S. Ling, C. Roberts, C.J. Goodman, P. Li, R.M. Goodall, Monitoring vertical track irregularity from in-service railway vehicles, Proc. Inst. Mech. Eng. Part F J. Rail Rapid Transit. 221 (1) (2007) 75–88.
[9] S. Kraft, J. Causse, F. Coudert, An approach for the classification of track geometry defects, Dyn. Veh. Roads Tracks (August) (2016) 1135–1144.
[10] H. Guler, S. Jovanovic, G. Evren, Modelling railway track geometry deterioration, Proc. Inst. Civ. Eng. – Transp. 164 (2) (2011) 65–75.
[11] C. Higgins, X. Liu, Modeling of track geometry degradation and decisions on safety and maintenance: a literature review and possible future research directions, Proc. Inst. Mech. Eng. Part F J. Rail Rapid Transit. 232 (5) (2018) 1385–1397.
[12] CEN(European Committee for Standardization), EN 13848-2 Railway applications-Track – Track geometry quality-Part 2: Measuring systems-Track recording vehicles, 2018.
[13] Fugro, Pictures from Fugro Raildata. [Online]. Available: https://www.fugro.com/our-services/asset-integrity/raildata [accessed: 16-Nov-2018].
[14] R. Wienia, Combined aerial and train mounted lidar system provide a fast and innovative approach to surveying railway infrastructure and track geometry. International Conference Railway Engineering, 2015.

[15] E. van den Bosch, Validatie RILA – S & C module, 2009.
[16] H. Wang, V. Markine, X. Liu, Experimental analysis of railway track settlement in transition zones, Proc. Inst. Mech. Eng. Part F J. Rail Rapid Transit. (2017).
[17] J.N. Varandas, P. Holscher, M.A. Silva, Settlement of ballasted track under traffic loading: application to transition zones, Proc. Inst. Mech. Eng. Part F J. Rail Rapid Transit. 228 (3) (2013) 242–259.
[18] B. Indraratna, M. Babar Sajjad, T. Ngo, A. Gomes Correia, R. Kelly, Improved performance of ballasted tracks at transition zones: a review of experimental and modelling approaches, Transp. Geotech. (2019).
[19] A. Paixão, E. Fortunato, R. Calçada, Transition zones to railway bridges: track measurements and numerical modelling, Eng. Struct. 80 (2014) 435–443.
[20] L. Le Pen, G. Watson, W. Powrie, G. Yeo, P. Weston, C. Roberts, The behaviour of railway level crossings: insights through field monitoring, Transp. Geotech. 1 (4) (2014) 201–213.
[21] J.O. Hallquist, LS-DYNA theoretical manual, Livermore Software Technology Corporation, Livermore, CA, May 1998, 1998.
[22] A. Lundqvist, T. Dahlberg, Load impact on railway track due to unsupported sleepers, Proc. Inst. Mech. Eng. Part F J. Rail Rapid Transit. 219 (2) (2005) 67–77.
[23] H. Wang, V.L. Markine, Methodology for the comprehensive analysis of railway transition zones, Comput. Geotech. 99 (October 2017) (2018) 64–79.
[24] H. Wang, V. Markine, Corrective countermeasure for track transition zones in railways: adjustable fastener, Eng. Struct. 169 (2018).
[25] J.C.O. Nielsen, E.G. Berggren, A. Hammar, F. Jansson, R. Bolmsvik, Degradation of railway track geometry – correlation between track stiffness gradient and differential settlement, Proc. Inst. Mech. Eng. Part F J. Rail Rapid Transit. (2018) 1–12.
[26] E.T. Selig, J.M. Waters, Track Geotechnology and Substructure Management, Thomas Telford, 1994.
[27] J.C.O. Nielsen, X. Li, Railway track geometry degradation due to differential settlement of ballast/subgrade – numerical prediction by an iterative procedure, J. Sound Vib. 412 (2018) 441–456.